

Received February 16, 2019, accepted March 5, 2019, date of publication March 8, 2019, date of current version April 2, 2019.

Digital Object Identifier 10.1109/ACCESS.2019.2904010

Intermittently Nonlinear Impulsive Noise Mitigation and Doppler Shift Compensation in UWA-OFDM Systems

REZA BARAZIDEH¹, SOLMAZ NIKNAM¹, BALASUBRAMANIAM NATARAJAN¹, AND ALEXEI V. NIKITIN^{1,3}

¹Department of Electrical and Computer Engineering, Kansas State University, Manhattan, KS 66506, USA

²Wireless@VT, Bradley Department of Electrical and Computer Engineering, Virginia Tech, Blacksburg, VA 24061, USA

³Nonlinear LLC, Wamego, KS 66547, USA

Corresponding author: Reza Barazideh (rezabarazideh@ksu.edu)

This work was supported in part by the Kansas State University Open Access Publishing Fund.

ABSTRACT Impulsive noise (IN) and Doppler shift can significantly degrade the performance of orthogonal frequency-division multiplexing (OFDM)-based underwater acoustic (UWA) communication systems. In this paper, we propose a receiver structure that deals efficiently with both these channel impairments in a coded OFDM-based UWA system. First, an analog nonlinear preprocessor (ANP) is proposed to efficiently detect and mitigate IN in an analog domain. The proposed ANP exhibits intermittent nonlinearity when there is impulsivity. Next, the impact of IN on a two-step Doppler shift compensation approach is quantified. Specifically, the ability of the ANP to improve the robustness of Doppler shift compensation in the presence of IN is highlighted. The performance improvement of the proposed receiver is due to the fact that unlike the other nonlinear methods, the ANP is implemented in the analog domain where the outliers are still broadband and distinguishable. The simulation results also demonstrate the superior bit-error-rate (BER) performance of our approach relative to classic approaches that use blanking and/or clipping for IN mitigation.

INDEX TERMS Impulsive noise (IN), analog nonlinear preprocessor (ANP), orthogonal frequency-division multiplexing (OFDM), Doppler shift, underwater acoustic (UWA).

I. INTRODUCTION

Underwater acoustic (UWA) communication is the most widely used technique for transmission in shallow water environments due to the low attenuation of sound in water [1]. Limited bandwidth, multipath fading, significant Doppler shifts, and strong IN are the major channel impairments in UWA communications [1]–[4]. The slow speed of sound, platform motion and instability of water medium result in significant frequency-dependent Doppler shifts and fast channel variations [3], [5]. Fast time varying channel can limit the use of equalizers to compensate for frequency-selective fading. In order to cope with the frequency selectivity of the propagation channel, orthogonal frequency-division multiplexing (OFDM) has been proposed [6]. In fact, by ensuring flat fading in each subcarrier, OFDM simplifies the equalizer structure and provides robustness against time-varying

frequency-selective fading. While cyclic prefix (CP) or zero padding (ZP) is used to provide a guard interval between consecutive OFDM symbols to avoid inter-symbol interference (ISI) [7], inter-carrier-interference (ICI) limits the performance in the presence of frequency-dependent Doppler shifts [3]. A computationally efficient Doppler scaling factor estimation, based on preamble and postamble, is proposed in [8] for single carrier transmissions. Assuming the UWA channel has a common Doppler scaling factor on all propagation paths, Li *et al.* [3] extend the work in [8] and provide a two-step Doppler mitigation approach to deal with frequency-dependent Doppler shifts in OFDM system. In the first step a resampling technique is used to remove nonuniform Doppler effect [3] and then, in the second step, a high resolution uniform compensation of the residual Doppler is performed based on modification of the null subcarrier methods [9].

In addition, the UWA channel is rich in IN induced by snapping shrimp in shallow warm waters [10], [11] or manmade

The associate editor coordinating the review of this manuscript and approving it for publication was Miaowen Wen.

noise near the shores [12]. Since OFDM employs a larger symbol duration (i.e., narrowband subcarriers), the energy of IN is naturally spread over all subcarriers. While this provides some level of robustness against impulsivity, system performance can still degrade if IN power exceeds a certain threshold [13]. IN mitigation has been extensively explored in prior efforts in wired and wireless communications. The impact of channel coding on IN cancelation has been investigated in [14]. It has been shown that unassisted coding can not fully alleviate the detrimental impact of severe IN in OFDM systems and using IN mitigation approach is inevitable [15].

In general, IN mitigation techniques in OFDM system can be divided into two classes. In the first class, the sparsity of the IN and the structure of OFDM signal are exploited [10]. In this class, first, an estimation of the IN is derived from the measurement on the null and/or pilot subcarriers, and then the estimated IN is subtracted from the received signals. For example, compressive sensing (CS) techniques are used to estimate IN by measurements on null subcarriers of OFDM [16], [17]. A sparse recovery based on sparse Bayesian learning (SBL) approach is provided in [18] and [19]. In [20], a combination of factor-graph-based receiver and message-passing technique is proposed to mitigate IN. However, the spectral efficiency of the CS-based methods need to improve since many OFDM subcarriers are nulled for measurements.

In the second class of IN mitigation techniques, high amplitude and short duration of the IN is considered as the main parameters for IN detection and cancelation. Conventional memoryless nonlinear approaches such as blanking and clipping are the most common methods in this class [21]. A combination of blanking and clipping [22] and multiple-threshold blanking/clipping [23] are proposed to improve the performance of blanking and clipping at extra computational complexity cost. A peak-to-average power ratio (PAPR) reduction technique along with nonlinear optimization search to find the optimal threshold for blanking/clipping is proposed in [24]. The performance of threshold-based nonlinear approaches is highly sensitive to the thresholds which are usually derived experimentally. In [25], a threshold optimization method based on Neyman-Pearson criterion is proposed. As shown in [21], the performance of all these methods degrades dramatically in severe impulsive environment.

Doppler shift compensation and IN mitigation in UWA systems can be performed sequentially one after another or jointly. An iterative joint Doppler shift and IN estimation based on nonlinear least squares (LS) formulation is proposed in [4], which is computationally complex. Bandwidth reduction in the process of analog-to-digital conversion (ADC) is the main drawback of all these digital nonlinear approaches [26], [27]. In [26], an Adaptive Nonlinear Differential Limiter (ANDL) is proposed to improve the bit-error-rate (BER) performance of uncoded OFDM-based powerline communication (PLC) systems in additive noise channel. A practical implementation of Adaptive Canonical Differential Limiter (ACDL) is studied in [27] to compensate

the IN in uncoded OFDM-based PLC systems. The output signal to noise ratio (SNR) and consequently the BER of the linearized ANDL is analytically quantified in [28].

In this paper, we investigate the performance of the analog nonlinear preprocessor (ANP) in the coded OFDM-based UWA channel. The proposed ANP offers a compromise between clipping and blanking in response to the impulsivity level which is determined based on outlier amplitude. Unlike our previous works [26]–[28], which are based on uncoded OFDM in additive noise channel, in this work coding, fading channel, and Doppler shift in the presence of IN are considered to model a realistic channel in UWA systems. Once the IN is mitigated by ANP in analog domain, the Doppler shift compensation and channel estimation can be accomplished by using null and pilot subcarriers, respectively, in the digital domain. We compare our proposed approach to the conventional methods such as blanking and clipping and highlight the advantage of the ANP for IN suppression. Simulation results show improvement in BER, due to the fact that, unlike classic IN mitigation methods, ANP is implemented in the analog domain where the outliers are still broadband and distinguishable.

The remainder of this paper is organized as follows. Section II describes the transmitter, channel, and noise models. Section III details the proposed receiver structure. Section IV presents simulation results and, finally, conclusions are drawn in Section V.

A. NOTATIONS

$Re(\cdot)$ denotes the real part of a complex number. $\delta(\cdot)$ and $\theta(\cdot)$ represent the Dirac delta and Heaviside unit step functions, respectively. Bold upper/lower-case letters denote matrices/column vectors; $(\cdot)^T$ and $(\cdot)^H$ denote the transpose and Hermitian of matrices, respectively. Finally, $\min(\cdot)$ and $\mathbb{E}[\cdot]$ are used to denote the minimum value and the expected value of the argument, respectively.

II. TRANSMITTER, CHANNEL, AND NOISE MODELS

A. TRANSMITTER MODEL

Fig. 1 shows a simplified block diagram of the coded OFDM-based UWA system considered in this work. At the transmitter, information bits are channel coded and then the encoded bits are interleaved. Subsequently, the interleaved data is modulated and passed through an inverse discrete Fourier transform (IDFT) module to generate OFDM symbols over orthogonal subcarriers. A cyclic prefix (CP) is inserted at the beginning of each OFDM symbol. Finally, the OFDM symbols are shaped by a root raised cosine (RRC) waveform with roll-off factor η and transmitted through the channel.

Let T and T_g denote the OFDM symbol duration and the length of the guard interval, respectively. The subcarrier spacing is $\Delta f=1/T$ and the total OFDM block duration is $T_{bl}=T+T_g$. Therefore, an OFDM signal with N subcarriers has the signal bandwidth of $B_s \approx N \Delta f$ and its k^{th} subcarrier is

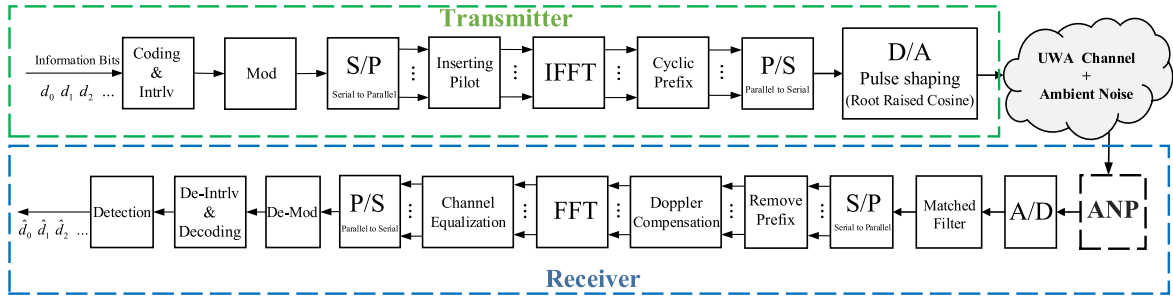


FIGURE 1. System model block diagram.

located at the frequency

$$f_k = f_c + k \Delta f, \quad k = -\frac{N}{2}, \dots, \frac{N}{2} - 1, \quad (1)$$

where f_c is the carrier frequency. In general, an OFDM symbol can be constructed with M non-data subcarriers and $N - M$ data subcarriers. The non-data subcarriers are either pilots for channel estimation and synchronization, or nulled for spectral shaping and ICI reduction. Let the nonoverlapping sets of data, pilot, and null subcarriers be defined as S_D , S_P , and S_N , respectively. Therefore, the transmitted passband analog signal envelope in time domain can be expressed as

$$\tilde{s}(t) = 2\operatorname{Re} \left\{ \sum_{k \in S_A} s_k e^{j2\pi f_k t} p(t) \right\}, \quad 0 < t < T_{bl} \quad (2)$$

where $S_A = S_D \cup S_P$ represents the set of active subcarriers, s_k is the modulated symbol on the k^{th} subcarrier, and $p(t)$ denotes RRC pulse shaping filter.

B. CHANNEL MODEL

The underwater acoustic channel can be modeled as a linear time-varying system which is described by the channel impulse response [3], [8]

$$c(\tau; t) = \sum_p b_p(t) \delta(\tau - \tau_p(t)), \quad (3)$$

where $b_p(t)$ and $\tau_p(t)$ are the time-varying amplitude and delay of the p^{th} multipath component, respectively. Assuming the signal duration is short compared to the coherence time of the channel, the following assumptions may be adopted [3], [4].

- Assumption 1): The delay variation can be approximated by its first-order Taylor series expansion

$$\tau_p(t) \approx \tau_p - a_p t, \quad (4)$$

where τ_p and a_p are the delay and Doppler scaling factor of the p^{th} path, respectively. In general different paths have different Doppler scaling factor; but, if the Doppler fluctuations remain relatively constant over a signal period (T_{bl}), the Doppler scaling factor can be considered as a constant value $a_p = a$ for all paths.

- Assumption 2): The path amplitudes b_p , and the delays τ_p are constant over T_{bl} . This is a reasonable assumption as channel coherence time is on the order of seconds and usually larger than the duration of a typical OFDM symbol in UWA system [3].

Based on assumptions 1 and 2, the received passband signal which is the convolution of the transmitted signal with the channel impulse response in the presence of IN, is given by

$$\begin{aligned} \tilde{x}(t) &= \int \sum_p A_p \delta(\tau - (\tau_p - at)) \tilde{s}(t - \tau) d\tau + \tilde{n}(t) \\ &= \sum_p A_p \tilde{s}((1+a)t - \tau_p) + \tilde{n}(t), \end{aligned} \quad (5)$$

where $\tilde{n}(t)$ is passband ambient noise which is dominated by snapping shrimp IN. The equivalent baseband received signal $x(t)$ corresponds to

$$\begin{aligned} x(t) &= \sum_{k \in S_A} \left\{ s_k e^{j2\pi(a f_k + k \Delta f) t} \right. \\ &\quad \left[\sum_p A_p e^{-j2\pi k f_k \tau_p} p(t + at - \tau_p) \right] \} + n(t) \\ &= x_s(t) + n(t), \end{aligned} \quad (6)$$

where $x_s(t)$ and $n(t)$ are desired signal and ambient noise in baseband, respectively.

C. AMBIENT NOISE MODEL

We assume that the passband ambient noise is dominated by the IN produced by snapping shrimp. On one hand, the main component of a pressure pulse generated by a snap is a short-duration (of order of a few microseconds or smaller) unipolar peak with rapid rise and fall [29]. On the other hand, a particular time-domain shape of the observed noise impulse due to a snap will largely depend on the combined filtering effect of the media, the hydrophone and its preamplifier, and the analog filtering ahead of ADC, which together can be viewed as an effect of an analog bandpass filter. Thus, since the raw duration of the snap is small (with significant energy content well beyond 100 kHz), this time domain shape would mainly resemble the impulse response of such analog bandpass filter. If the analog front end (including the hydrophone and its preamplifier) were carefully engineered to have a

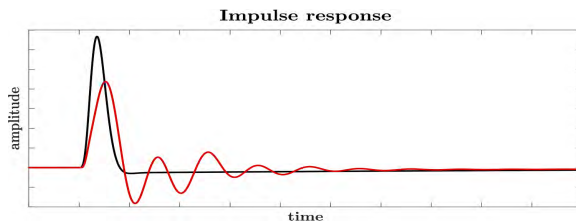


FIGURE 2. Impulse response of analog bandpass filter. (Black line is Bessel response).

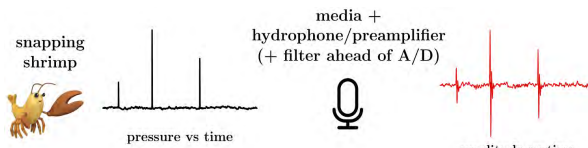


FIGURE 3. IN model.

response of a Bessel filter, the wave shape of the snap in the filters passband would be preserved and it would mainly look like a sharp unipolar peak followed by a slow undershoot. However, the filtering in a typical UWA communication system would be tailored for communications purposes and would not normally target the snapping shrimp noise shape preservation [30]. As the result, the analog impulse response in such a system is likely contain multiple undershoots and overshoots, as illustrated in Fig. 2, and the appearance of the IN produced by snapping shrimp may differ significantly from the original pressure profile, as illustrated in Fig. 3. Additional variations among the observed IN dime-domain appearances will be due to environmental effects, background noise contribution, changes in the media properties along the propagation path, and variations among the shrimp species. Therefore, in this paper we will adopt two commonly used models for ambient noise in UWA environments as outlined below.

Bernoulli-Gaussian Model: Ambient noise can be considered as composition of thermal noise $w(t)$ and IN $i(t)$. Here, $w(t)$ is complex Gaussian noise and $i(t)$ is modeled as a Poisson shot noise that consists of short duration high power impulses with random arrivals and corresponds to

$$i(t) = v(t) \sum_{k=1}^{\infty} B_k [\theta(t - t_k) - \theta(t - t_k - \tau_{as})]. \quad (7)$$

Here, $v(t)$ is a complex white Gaussian noise process with zero mean; B_k represent the amplitude of k^{th} pulse; t_k is the arrival time of a Poisson process with parameter λ , and τ_{as} denotes the duration of the IN. Although (7) captures a burst IN in analog domain with random amplitude, it also can represent Bernoulli-Gaussian (BG) IN model in time duration T with average success probability P_i given by

$$P_i = \left[\sum_{k=0}^{\infty} \frac{e^{-\lambda T} (\lambda T)^k}{k!} k \tau_{as} \right] / T$$

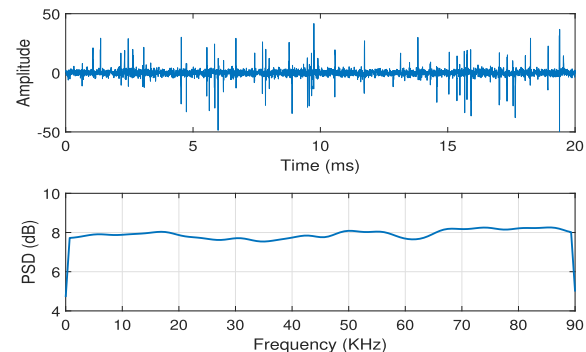


FIGURE 4. Ambient noise with BG impulsive noise.

$$\begin{aligned} &= \lambda \tau_{as} \left[\sum_{k=1}^{\infty} \frac{e^{-\lambda T} (\lambda T)^{k-1}}{(k-1)!} \right] \\ &= \lambda \tau_{as} \left[\sum_{k=0}^{\infty} \frac{e^{-\lambda T} (\lambda T)^k}{k!} \right] \\ &= \lambda \tau_{as}. \end{aligned} \quad (8)$$

The resulting time and frequency domain representation of ambient noise with BG underlying impulsive noise is depicted in Fig. 4.

Alpha sub-Gaussian Noise with memory: In general ambient noise can be modeled based on heavy-tailed distributions as they assign large probability to outliers. It has been shown that symmetric alpha-stable (S α S) family of distributions have a good fit to ambient noise in warm shallow waters, which is impulsive and bursty [10]. In practice, this kind of noise is not white and it is not possible to exploit white symmetric alpha-stable noise (WS α SN) model, which only incorporates the amplitude distribution of the noise process without considering the dependency between adjacent noise samples [10], [31]. Therefore, we model the ambient noise as stationary alpha sub-Gaussian noise with memory order m (α SGN(m)) [11], [31] which considers both the amplitude distribution and dependency across the noise samples.

Let n_k be the random samples of an α SG(m) process at index k . Then $\mathbf{n}_{k,m} = [n_{k-m}, n_{k-m+1}, \dots, n_k]^T$ is a $(m+1)$ -dimensional α SG random vector for all $k \in \mathbb{Z}$ and can be expressed as [11], [31]

$$\mathbf{n}_{k,m} = A_k^{1/2} \mathbf{G}_{k,m}, \quad (9)$$

where $A \sim S(\alpha/2, 1, 2(\cos(\pi\alpha/4))^2, 0)$ is a stable random variable with parameter α and $\mathbf{G}_{k,m} = [G_{k-m}, G_{k-m+1}, \dots, G_k]^T$ is Gaussian with distribution $\mathcal{N}(\mathbf{0}, \mathbf{R}_m)$ and $\mathbf{R}_m \in \mathbb{R}^{(m+1) \times (m+1)}$. Since α SGN(m) is stationary, the covariance matrix $R_m = [r_{ij}]$ is independent of k and symmetric Toeplitz matrix, which is also positive-semidefinite [31]. The resulting time and frequency domain representation of ambient noise with α SGN(4) underlying impulsive noise is illustrated in Fig. 5. Note that, WS α SN is a special case of α SGN(m) with $m = 0$. More details on the α SGN(m) model can be found in [11] and [32]. Although, the

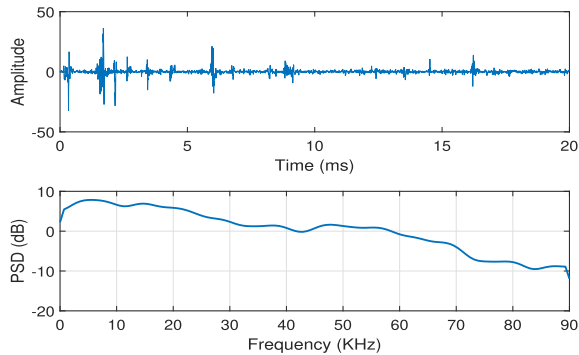


FIGURE 5. Ambient noise with α SGN(4) impulsive noise.

α SGN(m) in [11] model the ambient noise in digital domain, one can find the analog counter part of this model by exploiting interpolation techniques.

III. RECEIVER STRUCTURE

The block diagram of the proposed receiver is shown in Fig. 1. Here, in order to deal with the IN, the ANP module is implemented in analog domain before the ADC, as a front end preprocessor. In addition, the Doppler compensation is performed after cyclic prefix removal. This is followed by frequency domain equalization that depends on channel estimation. Viterbi soft decoding is used to decode the demodulated signal and then detection is performed based on the modulation scheme used. In this section, we first introduce the proposed ANP. Secondly, the Doppler effect compensation technique is introduced and, finally, the channel estimation approach is highlighted.

A. ANP DESIGN

It is well known that locally optimum detection of signals in non-Gaussian noise exploits nonlinear kernels [32]. For easier implementation we propose a suboptimal threshold-based nonlinear suppressor that is linear when there is no outliers. ANP is an intermittently nonlinear preprocessor that goes to nonlinear regime in response to incoming outliers. The general block diagram of ANP is depicted in Fig. 6 which is fully compatible with existing linear receivers and can be inserted as a front end filter to current receivers. Here, $x(t)$ and $y(t)$ are the input and output of the ANP, respectively.

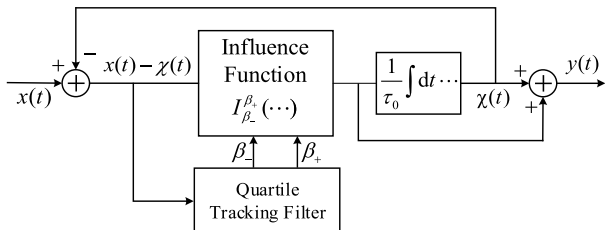


FIGURE 6. Block diagram of generalized ANP.

The output of the ANP can be represented as

$$\begin{cases} y(t) = \chi(t) + \tau_0 \dot{\chi}(t) \\ \dot{\chi}(t) = \frac{1}{\tau_0} \mathcal{I}_{\beta_-}^{\beta_+}(x(t) - \chi(t)), \end{cases} \quad (10)$$

where $\tau_0 = 1/(4\pi B_s)$ is fixed time constant, $\dot{\chi}(t)$ denotes the first time derivative of $\chi(t)$, and $\mathcal{I}_{\beta_-}^{\beta_+}(x)$ is the influence function. We will require that $\mathcal{I}_{\beta_-}^{\beta_+}(x)$ is effectively linear for $\beta_- \leq x \leq \beta_+$, and its absolute value monotonically decays to zero for x outside of the range $[\beta_-, \beta_+]$. For example, particular realization of influence function for ANP can be given by

$$\mathcal{I}_{\beta_-}^{\beta_+}(x) = \begin{cases} \beta_+ \exp\left(-\gamma \left(\frac{x - \beta_+}{\Delta\beta}\right)^2\right), & x > \beta_+ \\ \beta_- \exp\left(-\gamma \left(\frac{\beta_- - x}{\Delta\beta}\right)^2\right), & x < \beta_- \\ x, & \text{otherwise,} \end{cases} \quad (11)$$

where $\Delta\beta = \beta_+ - \beta_-$ and γ is a constant that determines how fast the proposed influence function transitions from clipping ($\gamma = 0$) to blanking ($\gamma \rightarrow \infty$). In other words, this influence function changes the nonlinearity from clipping to blanking based on the amplitude of incoming signal. The relation between input and output of the influence function for different values of γ is illustrated in Fig. 7. Note that, the value of γ will differ based on the application and the underlying IN model but as shown in the result section of this paper a simply choice of $\gamma = 1$ provides satisfactory performance. The expression in (11) demonstrates that ANP aggressively deprecate high amplitude IN and the nonlinear response of the ANP suppresses the magnitude of the respective outliers in the output signal. On the other hand, as follows from (10), when $\beta_- \leq x(t) - \chi(t) \leq \beta_+$ the output $y(t)$ of the ANP simply equals to its input $x(t)$ which means the proposed ANP does not harm the desired signal when there is no IN. Therefore, a proper selection of sensitivity range $[\beta_-, \beta_+]$ ensures the quality of the ANP. In this work, an effective value of the interval $[\beta_-, \beta_+]$ is obtained by using Quartile Tracking Filter (QTF) [27] as shown in Fig. 6. The QTF

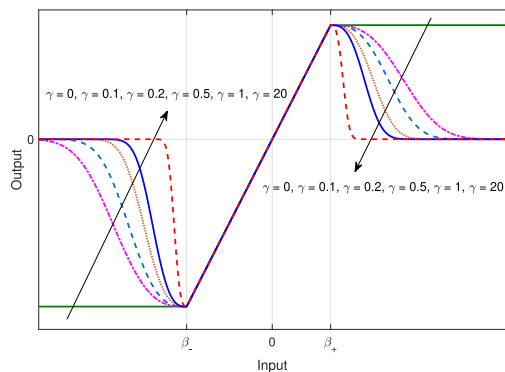


FIGURE 7. Relation between input and output of influence function.

uses Tukey's range [33], which is a linear combination of the first (Q_1) and the third (Q_3) quartiles of the difference signal $x(t) - \chi(t)$ and is given by

$$[\beta_-, \beta_+] = [Q_1 - \beta_0(Q_3 - Q_1), Q_3 + \beta_0(Q_3 - Q_1)], \quad (12)$$

where β_0 is a constant coefficient of order unity (e.g. $\beta_0 = 3$). Note that the difference signal $x(t) - \chi(t)$ provides an estimation of incoming time varying impulsive noise. We direct the reader to [27] and [34] for details on QTF and obtaining the quartile values $Q_1(t)$ and $Q_3(t)$ in analog domain.

B. DOPPLER EFFECT COMPENSATION

The ANP is followed by cyclic prefix removal and then the Doppler effect in the signal can be mitigated through a two step Doppler compensation technique described in [3]. The nonuniform Doppler effect of the received signal is removed through polyphase-interpolation-based resampling factor \hat{a} , resulting in a resampled signal. The estimate \hat{a} of the Doppler scaling factor a , is calculated by comparing the time duration of the received packet \hat{T}_{rx} with the known time duration of the transmitted packet T_{tx} , given by [8]

$$\hat{T}_{rx} = \frac{T_{tx}}{1 + \hat{a}} \Rightarrow \hat{a} = \frac{T_{tx}}{\hat{T}_{rx}} - 1, \quad (13)$$

where the received packet time duration \hat{T}_{rx} is estimated in the receiver by cross-correlating the received signal with the known preamble and postamble. After IN mitigation and resampling by factor \hat{a} , the received resampled baseband signal $r[n]$ in digital domain can be expressed as

$$\begin{aligned} r[n] &= y \left[\left(\frac{n}{1 + \hat{a}} \right) T_c \right] \\ &\approx e^{j2\pi\epsilon n T_c} \{ s[n] * h_{eff}[n] + v[n] \}, \end{aligned} \quad (14)$$

where $h_{eff}[n]$ and $v[n]$ are the effective channel impulse response and residual noise, respectively. Here, ϵ denotes the residual Doppler effect that can be considered to be the same for all subcarriers. Note that ϵ is similar to the carrier frequency offset (CFO) in radio frequency (RF) communication. The compensation of the CFO in (14) can be performed by

$$\begin{aligned} d[n] &= r[n] e^{-j2\pi\hat{\epsilon}n T_c} \\ &\approx s[n] * h_{eff}[n] + v[n], \end{aligned} \quad (15)$$

where $\hat{\epsilon}$ is the estimated value of CFO and is generated for each OFDM block. The CFO estimation is done by minimizing the leakage energy in the null subcarriers. In fact, if the receiver compensates the CFO, the null subcarriers will not see the ICI spilled over from neighboring subcarriers. Define the cost function

$$J(\epsilon) = \sum_{k \in S_N} \left| \mathbf{f}_k^H \Gamma^H(\epsilon) \mathbf{r} \right|^2, \quad (16)$$

where, \mathbf{f}_k , Γ , and \mathbf{r} can be defined as

$$\mathbf{f}_k := \left[1, e^{j2\pi k/N}, \dots, e^{j2\pi k(N-1)/N} \right]^T$$

$$\begin{aligned} \Gamma(\epsilon) &:= \text{diag} \left(1, e^{j2\pi T_c \epsilon}, \dots, e^{j2\pi T_c (N-1) \epsilon} \right) \\ \mathbf{r} &:= [r(0), \dots, r(N-1)]^T. \end{aligned} \quad (17)$$

Considering (17), by sampling with rate B_s , we obtain N samples for each OFDM block. Therefore, the estimate of ϵ is given by

$$\hat{\epsilon} = \arg \min_{\epsilon} J(\epsilon), \quad (18)$$

which can be solved by a 1-D search for ϵ or using standard gradient method [9]. The mean square error (MSE) is used as a measure to quantify the performance of the CFO compensation technique in the IN environment. Thus, the MSE of Doppler compensation approach corresponds to

$$MSE_{CFO} = \mathbb{E} \left[(\epsilon - \hat{\epsilon})^2 \right]. \quad (19)$$

C. CHANNEL ESTIMATION

In order to estimate the channel response at the receiver, pilot subcarriers are used. Define the channel frequency response as

$$C(f) := \sum_p b_p e^{-j2\pi f \tau_p}, \quad (20)$$

the received signal in the k^{th} subcarrier is given by

$$r_k = \mathbf{f}_k^H \Gamma^H(\hat{\epsilon}) \mathbf{r} = s[k] H[k] + v_k, \quad (21)$$

where $H[k] = C(f_k)$ is the channel frequency response at k^{th} subcarrier and v_k is the residual noise. Given that the channel has $L + 1$ taps in discrete time, the channel estimation can be done using N_p pilot tones (at subcarrier indices $\{p_1, \dots, p_{N_p}\} \in S_p$) based on least squares (LS) method as long as $N_p \geq L + 1$. Assuming that ISI is eliminated by the CP or guard interval, we obtain

$$\mathbf{r}_p = \mathbf{D}_s \mathbf{F} \mathbf{h} + \mathbf{v}, \quad (22)$$

where

$$\begin{aligned} \mathbf{r}_p &:= [r_{p_1}, \dots, r_{p_{N_p}}] \\ \mathbf{D}_s &:= \text{diag}(s_{p_1}, \dots, s_{p_{N_p}}) \\ \mathbf{h} &:= [h_0, \dots, h_L] \\ \mathbf{F} &:= \begin{bmatrix} 1 & e^{-j\frac{2\pi}{N} p_1} & \dots & e^{-j\frac{2\pi}{N} p_1 L} \\ \vdots & \vdots & \ddots & \vdots \\ 1 & e^{-j\frac{2\pi}{N} p_{N_p}} & \dots & e^{-j\frac{2\pi}{N} p_{N_p} L} \end{bmatrix}. \end{aligned} \quad (23)$$

For the sake of simplicity and avoiding matrix inversion operation, we assume that pilot symbols are equally spaced within N subcarriers and they are PSK signals with unit amplitude. Thus, the matrix-vector representation of the equivalent system is obtained by

$$\begin{aligned} \mathbf{F}^H \mathbf{F} &= N_p \mathbf{I}_{L+1} \\ \mathbf{D}_s^H \mathbf{D}_s &= \mathbf{I}_{N_p}, \end{aligned} \quad (24)$$

and the LS estimate of \mathbf{h} is represented by

$$\hat{\mathbf{h}}_{LS} = \frac{1}{N_p} \mathbf{F}^H \mathbf{D}_s^H \mathbf{r}_p. \quad (25)$$

TABLE 1. Simulation Parameters.

Parameters	Values
Bandwidth (B_s)	6 kHz
Carrier Frequency (f_c)	17 kHz
No. of Subcarriers (N)	1024
Subcarrier Spacing (Δf)	5.88 Hz
Symbol Duration (T)	170.7 ms
Guard Interval (T_g)	79.3 ms
ADC Sampling Interval (T_c)	20.8 μ s
Modulation Scheme	QPSK
Channel Length (L)	10
Convolution Code Rate (CR)	1/2
Code Constraint Length	7
Generator Polynomial	[171,133]
Roll-off Factor (η)	0.25

Having time domain channel estimate \hat{h}_{LS} , the estimate of the channel at all subcarriers is obtained by [35]

$$\hat{H}[k] = \sum_{l=0}^L \hat{h}_l e^{\frac{-j2\pi lk}{N}}. \quad (26)$$

In order to quantify the performance of channel estimation, the relative MSE of channel estimation corresponds to

$$MSE_{CE} = \mathbb{E} \left[\frac{(\mathbf{h} - \hat{\mathbf{h}}_{LS})^\mathcal{H} (\mathbf{h} - \hat{\mathbf{h}}_{LS})}{\mathbf{h}^\mathcal{H} \mathbf{h}} \right]. \quad (27)$$

IV. SIMULATION RESULTS

In this section, an UWA system with QPSK modulation in the presence of IN is studied. The BER performance is used to compare the proposed ANP with other conventional approaches such as blanking and clipping. In addition, the MSE of Doppler compensation and channel estimation are investigated to highlight the impact of IN mitigation in estimation fidelity.

For a quick reference, the simulation parameters of the considered coded OFDM system in UWA channels are listed in Table 1. A total of 1024 subcarriers are used with 672 carrying data, 256 pilot, and 96 null subcarriers. Channel estimation is done based on pilot subcarriers which are equally spaced between 1024 subcarriers. The CFO is compensated based on null subcarriers which are placed between data and pilot subcarriers. To emulate analog signals in the simulation, the digitization rate is chosen to be significantly higher (by about two orders of magnitude) than the ADC sampling interval T_c . A 10-path fading channel is considered with path arrival times following a Poisson distribution with mean 1 ms. The path amplitudes are Rayleigh distributed with exponentially decreasing average power about 30 dB between the first and last path. The Doppler shift ϵ is uniformly distributed in $[-\Delta f/2, \Delta f/2]$. The considered covariance matrices for α SGN(m) model with $m = 4$ and $m = 1$ are given by

$$\mathbf{R}_4 = \begin{bmatrix} 1.0000 & 0.5804 & 0.2140 & 0.1444 & -0.0135 \\ 0.5804 & 1.0000 & 0.5804 & 0.2140 & 0.1444 \\ 0.2140 & 0.5804 & 1.0000 & 0.5804 & 0.2140 \\ 0.1444 & 0.2140 & 0.5804 & 1.0000 & 0.5804 \\ -0.0135 & 0.1444 & 0.2140 & 0.5804 & 1.0000 \end{bmatrix},$$

$$\mathbf{R}_1 = \begin{bmatrix} 1.0 & 0.7 \\ 0.7 & 1.0 \end{bmatrix}. \quad (28)$$

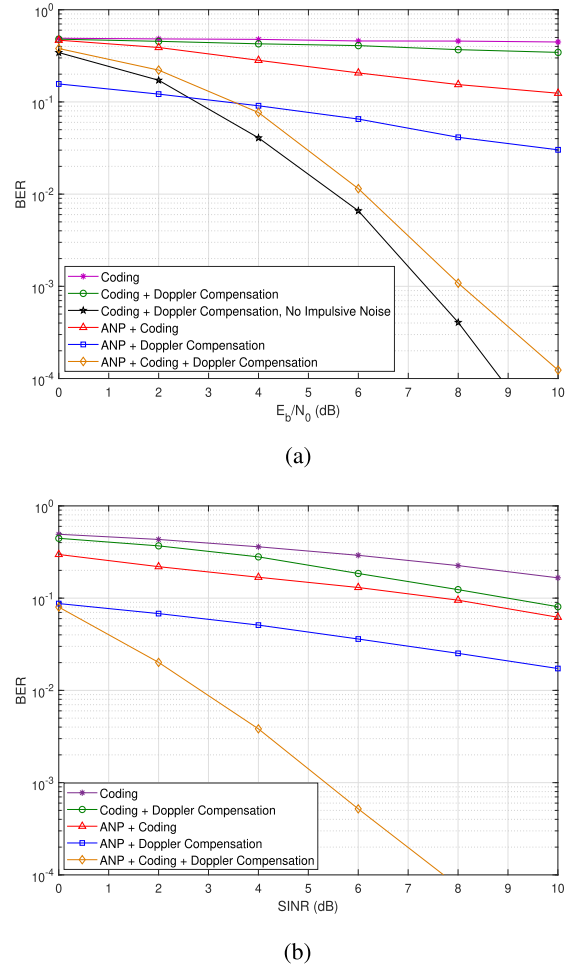
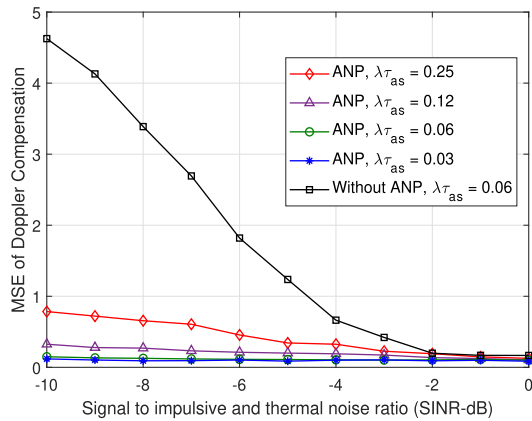
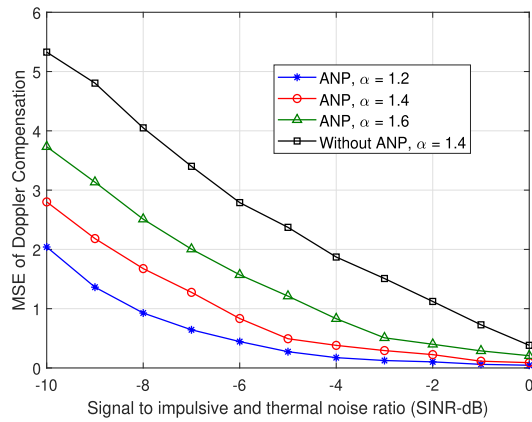


FIGURE 8. BER performance for different model of IN. (a) BG IN, SIR = 0 dB, $\tau_{as} = 10 \mu s$, $\lambda \tau_{as} = 0.03$. (b) α SGN(m) IN, $\alpha = 1.5$, $m = 4$.

The importance of IN mitigation in the OFDM-based receiver chain under two different settings (i) BG noise with $SIR = 0$ dB, $\lambda \tau_{as} = 0.03$, and (ii) α SGN(m) noise with $\alpha = 1.5$, and memory $m = 4$, are shown in Fig. 8a and Fig. 8b, respectively. As is evident from Fig. 8, coding alone can not deal with IN in an OFDM system. This is because of the fact that the power of IN is spread over the entire OFDM symbol which makes error correction impossible. Fig. 8 also shows that Doppler compensation in UWA channel is inevitable either with or without IN mitigation techniques. From Fig. 8 it is obvious that the best performance is achieved when the IN is suppressed by ANP with effective coding and Doppler compensation. The effect of ANP on the quality of the Doppler compensation and channel estimation are shown in Fig. 9 and Fig. 10, respectively. Fig. 9a and Fig. 9b demonstrates the effect of ANP on the MSE of Doppler compensation technique for both BG and α SGN(m) IN models, respectively. As shown in Fig. 9, ANP improves the quality of CFO compensation technique in different levels of impulsivity. The MSE of channel estimation in both BG and α SGN(m) are shown in Fig. 10a and Fig. 10b, respectively. As we are interested in quantifying the impact of IN on channel estimation, the frequency offset is set to



(a)



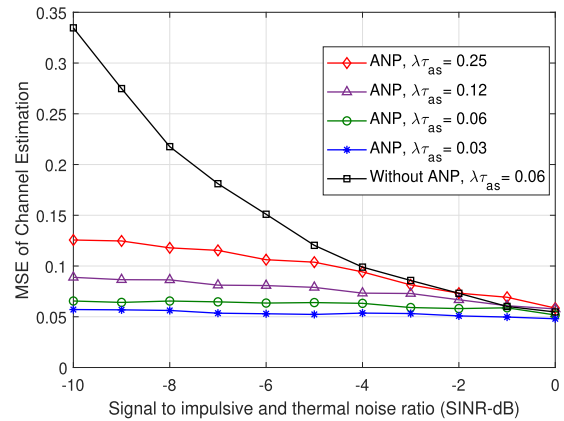
(b)

FIGURE 9. MSE of Doppler compensation. (a) BG IN, $E_b/N_0 = 2$ dB, $\tau_{as} = 10\mu s$. (b) α SGN(m) IN, $m = 4$.

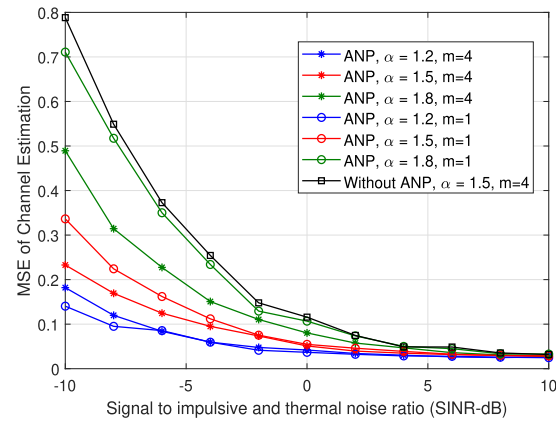
zero for the simulations in Fig. 10. As illustrated in Fig. 10, the fidelity of channel estimation technique remains good with ANP even in the presence of severe impulsivity. It is important to remember that both Doppler compensation and channel estimation are done in the frequency domain where the power of IN is spread over all OFDM subcarriers. Thus, without the ANP, the MSE is more severely impacted by the power of IN rather than its occurrence frequency.

In the following, we compare the performance of the ANP with two digital approaches of IN mitigation namely blanking (BLN) and clipping (CLP). Note that in all simulations, (i) the optimum thresholds for blanking and clipping are found based on an exhaustive numerical search, (ii) the sensitivity range $[\beta_-, \beta_+]$ for ANP is determined based on expression (12) with low computational complexity, and (iii) coding, Doppler compensation, and channel estimation are considered in all receivers except where it is mentioned otherwise.

Fig. 11 compares the BER performance of all three receivers in BG noise for different levels of impulsivity. Fig. 11 shows that in BG IN model, blanking and clipping are very vulnerable to the occurrence frequency of IN and their performance is poor in high impulsive environments.



(a)



(b)

FIGURE 10. MSE of channel estimation. (a) BG IN, $E_b/N_0 = 2$ dB, $\tau_{as} = 10\mu s$. (b) α SGN(m) IN.

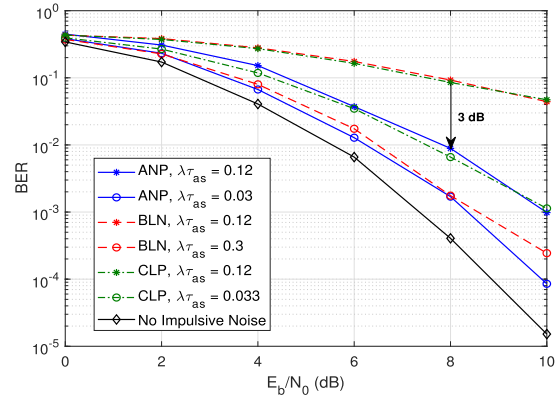
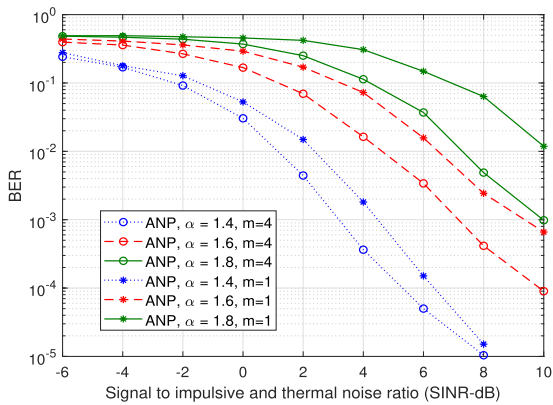
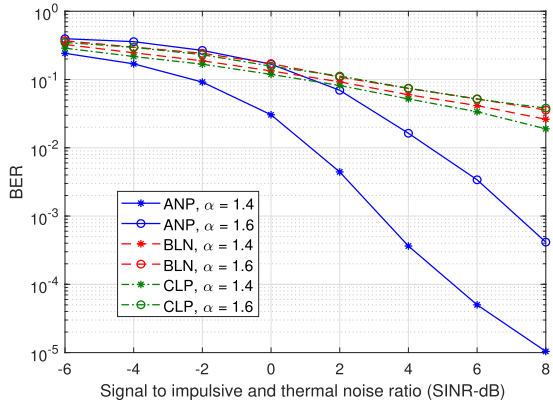
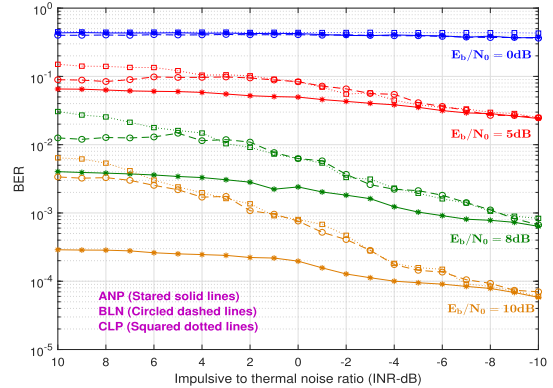


FIGURE 11. BER comparison of ANP, BLN, and CLP in BG noise for different values of λ . SIR = 0 dB, $\tau_{as} = 10\mu s$.

Although, the performance loss of the ANP with increasing the impulsivity level is also noticeable, it still outperforms other approaches in all scenarios. For example, at $E_b/N_0 = 8$ dB, ANP provides 3 dB gain relative to blanking and clipping for $\lambda\tau_{as} = 0.12$. The BER performance of ANP in case of α SGN(m) model for different values of α and memory size is shown in Fig. 12. According to α SGN(m) model, a smaller α denotes more impulsive environment which means at a

FIGURE 12. BER performance of ANP in α SGN(m) noise.FIGURE 13. BER comparison of ANP, BLN, and CLP in α SGN(m) noise, $m = 4$.FIGURE 14. BER comparison of ANP, BLN, and CLP in BG noise for different values of E_b/N_0 . $\tau_{as} = 10\mu s$, $\lambda\tau_{as} = 0.06$.

given SINR the power of outliers is more than the power of thermal noise. Therefore, as shown in Fig. 12 we have better performance for lower values of α because ANP is able to suppress the outlier more efficiently. Fig. 13 shows that the ANP considerably outperforms other methods. The potency of ANP in reducing the power of IN in the signal passband is due to the fact that, unlike other nonlinear methods, ANP is implemented in the analog domain where the outliers are still broadband and distinguishable.

Fig. 14 illustrates the BER performance of all three IN mitigation approaches in case of BG model for various IN

to thermal noise ratios (INR) in baseband. As can be seen in Fig. 14, all approaches provide effectively equivalent performance when thermal noise dominates the IN (right side of Fig. 14). However, the ANP shows its advantage when IN is dominant, specially at high SNR (SNR greater than 5 dB). Therefore, in highly impulsive environment as shown in Fig. 14, ANP is highly preferable to other approaches.

V. CONCLUSION

In this work, we have investigated a novel method to mitigate the effect of impulsive noise (IN) and its impact on nonuniform Doppler shift compensation in the coded OFDM-based UWA systems. First, we suppress the IN by using an analog nonlinear preprocessor (ANP). Second, the Doppler shift compensation and channel estimation are performed based on the measurements on OFDM null and pilot subcarriers, respectively. The results show that the proposed approach can provide significant improvement in BER performance of the UWA system in the presence of both strong impulsive component and nonuniform Doppler shift. In addition, the ANP-based approach outperforms other methods that use blanking or clipping for outlier suppression, specially at high levels of impulsivity. The potency of the ANP is due to the fact that unlike digital IN mitigation methods, ANP is implemented in the analog domain where the outliers are still broadband and distinguishable. It is worth mentioning that the efficiency of the proposed mitigation technique can be significantly increased by inserting the ANP even earlier in the analog part of the signal chain, preferably as a part of the hydrophones preamplifier, and by minimizing the pulse shape distortions caused by the filtering affects of the hydrophone and its preamplifier.

REFERENCES

- [1] M. Chitre, S. Shahabudeen, L. Freitag, and M. Stojanovic, "Recent advances in underwater acoustic communications & networking," in *Proc. OCEANS*, Sep. 2008, pp. 1–10.
- [2] D. B. Kilfoyle and A. B. Baggeroer, "The state of the art in underwater acoustic telemetry," *IEEE J. Ocean. Eng.*, vol. 25, no. 1, pp. 4–27, Jan. 2000.
- [3] B. Li, S. Zhou, M. Stojanovic, L. Freitag, and P. Willett, "Multicarrier communication over underwater acoustic channels with nonuniform Doppler shifts," *IEEE J. Ocean. Eng.*, vol. 33, no. 2, pp. 198–209, Apr. 2008.
- [4] X. Kuai, H. Sun, S. Zhou, and E. Cheng, "Impulsive noise mitigation in underwater acoustic OFDM systems," *IEEE Trans. Veh. Technol.*, vol. 65, no. 10, pp. 8190–8202, Oct. 2016.
- [5] M. Stojanovic, "Low complexity OFDM detector for underwater acoustic channels," in *Proc. OCEANS*, Sep. 2006, pp. 1–6.
- [6] J. A. C. Bingham, "Multicarrier modulation for data transmission: An idea whose time has come," *IEEE Commun. Mag.*, vol. 28, no. 5, pp. 5–14, May 1990.
- [7] B. Muquet, Z. Wang, G. B. Giannakis, M. D. Courville, and P. Duhamel, "Cyclic prefixing or zero padding for wireless multicarrier transmissions?" *IEEE Trans. Commun.*, vol. 50, no. 12, pp. 2136–2148, Dec. 2002.
- [8] B. S. Sharif, J. Neasham, O. R. Hinton, and A. E. Adams, "A computationally efficient Doppler compensation system for underwater acoustic communications," *IEEE J. Ocean. Eng.*, vol. 25, no. 1, pp. 52–61, Jan. 2000.
- [9] X. Ma, C. Tepedelenlioglu, G. B. Giannakis, and S. Barbarossa, "Non-data-aided carrier offset estimators for OFDM with null subcarriers: Identifiability, algorithms, and performance," *IEEE J. Sel. Areas Commun.*, vol. 19, no. 12, pp. 2504–2515, Dec. 2001.

- [10] M. A. Chitre, J. R. Potter, and S.-H. Ong, "Optimal and near-optimal signal detection in snapping shrimp dominated ambient noise," *IEEE J. Ocean. Eng.*, vol. 31, no. 2, pp. 497–503, Apr. 2006.
- [11] A. Mahmood and M. Chitre, "Modeling colored impulsive noise by Markov chains and alpha-stable processes," in *Proc. OCEANS-Genova*, May 2015, pp. 1–7.
- [12] J. A. Hildebrand, "Anthropogenic and natural sources of ambient noise in the ocean," *Marine Ecol. Prog. Ser.*, vol. 395, no. 5, pp. 5–20, 2009.
- [13] M. Ghosh, "Analysis of the effect of impulse noise on multicarrier and single carrier QAM systems," *IEEE Trans. Commun.*, vol. 44, no. 2, pp. 145–147, Feb. 1996.
- [14] D. Umehara, H. Yamaguchi, and Y. Morihiko, "Turbo decoding in impulsive noise environment," in *Proc. Global Telecommun. Conf.*, vol. 1, Nov./Dec. 2004, pp. 194–198.
- [15] G. Ndo, P. Siohan, M.-H. Hamon, and J. Horard, "Optimization of turbo decoding performance in the presence of impulsive noise using soft limitation at the receiver side," in *Proc. Global Telecommun. Conf.*, Nov./Dec. 2008, pp. 1–5.
- [16] T. Y. Al-Naffouri, A. A. Quadeer, and G. Caire, "Impulse noise estimation and removal for OFDM systems," *IEEE Trans. Commun.*, vol. 62, no. 3, pp. 976–989, Mar. 2014.
- [17] S. Liu, F. Yang, X. Wang, J. Song, and Z. Han, "Structured-compressed-sensing-based impulsive noise cancellation for MIMO systems," *IEEE Trans. Veh. Technol.*, vol. 66, no. 8, pp. 6921–6931, Aug. 2017.
- [18] J. Lin, M. Nassar, and B. L. Evans, "Impulsive noise mitigation in power-line communications using sparse Bayesian learning," *IEEE J. Sel. Areas Commun.*, vol. 31, no. 7, pp. 1172–1183, Jul. 2013.
- [19] S. Liu, F. Yang, J. Song, and Z. Han, "Block sparse Bayesian learning-based NB-IoT interference elimination in LTE-advanced systems," *IEEE Trans. Commun.*, vol. 65, no. 10, pp. 4559–4571, Oct. 2017.
- [20] M. Nassar, P. Schniter, and B. L. Evans, "A factor graph approach to joint OFDM channel estimation and decoding in impulsive noise environments," *IEEE Trans. Signal Process.*, vol. 62, no. 6, pp. 1576–1589, Mar. 2014.
- [21] S. V. Zhidkov, "Analysis and comparison of several simple impulsive noise mitigation schemes for OFDM receivers," *IEEE Trans. Commun.*, vol. 56, no. 1, pp. 5–9, Jan. 2008.
- [22] H. Oh and H. Nam, "Design and performance analysis of nonlinearity preprocessors in an impulsive noise environment," *IEEE Trans. Veh. Technol.*, vol. 66, no. 1, pp. 364–376, Jan. 2017.
- [23] N. Rožić, P. Banelli, D. Begušić, and J. Radić, "Multiple-threshold estimators for impulsive noise suppression in multicarrier communications," *IEEE Trans. Signal Process.*, vol. 66, no. 6, pp. 1619–1633, Mar. 2018.
- [24] K. Anoh, B. Adegbisi, K. M. Rabie, M. Hammoudeh, and H. Gacanin, "On companding and optimization of OFDM signals for mitigating impulsive noise in power-line communication systems," *IEEE Access*, vol. 5, pp. 21818–21830, 2017.
- [25] G. Ndo, P. Siohan, and M. H. Hamon, "Adaptive noise mitigation in impulsive environment: Application to power-line communications," *IEEE Trans. Power Del.*, vol. 25, no. 2, pp. 647–656, Apr. 2010.
- [26] R. Barazideh, B. Natarajan, A. V. Nikitin, and R. L. Davidchack, "Performance of analog nonlinear filtering for impulsive noise mitigation in OFDM-based PLC systems," in *Proc. IEEE Latin-Amer. Conf. Commun.*, Nov. 2017, pp. 1–6.
- [27] R. Barazideh, A. V. Nikitin, and B. Natarajan, "Practical implementation of adaptive analog nonlinear filtering for impulsive noise mitigation," in *Proc. IEEE Int. Conf. Commun. (ICC)*, May 2018, pp. 1–7.
- [28] R. Barazideh, B. Natarajan, A. V. Nikitin, and S. Niknam, "Performance analysis of analog intermittently nonlinear filter in the presence of impulsive noise," *IEEE Trans. Veh. Technol.*, to be published. doi: [10.1109/TVT.2019.2896924](https://doi.org/10.1109/TVT.2019.2896924).
- [29] M. W. Legg, A. J. Duncan, A. Zakhnich, and M. V. Greening, "Analysis of impulsive biological noise due to snapping shrimp as a point process in time," in *Proc. OCEANS-Europe*, Jun. 2007, pp. 1–6.
- [30] D. C. Bertilone and D. S. Killeen, "Statistics of biological noise and performance of generalized energy detectors for passive detection," *IEEE J. Ocean. Eng.*, vol. 26, no. 2, pp. 285–294, Apr. 2001.
- [31] A. Mahmood and M. Chitre, "Optimal and near-optimal detection in bursty impulsive noise," *IEEE J. Ocean. Eng.*, vol. 42, no. 3, pp. 639–653, Jul. 2017.
- [32] H. V. Poor, *An Introduction to Signal Detection Estimation*, 2nd ed. New York, NY, USA: Springer, 1994.
- [33] J. W. Tukey, *Exploratory Data Analysis*. Reading, MA, USA: Addison-Wesley, 1977.
- [34] A. V. Nikitin and R. L. Davidchack, "Adaptive approximation of feedback rank filters for continuous signals," *Signal Process.*, vol. 84, no. 4, pp. 805–811, Apr. 2004.
- [35] S. Coleri, M. Ergen, A. Puri, and A. Bahai, "Channel estimation techniques based on pilot arrangement in OFDM systems," *IEEE Trans. Broadcast.*, vol. 48, no. 3, pp. 223–229, Sep. 2002.



REZA BARAZIDEH received the B.Sc. degree in electrical engineering from the Amirkabir University of Technology (Tehran Polytechnic), Tehran, Iran, in 2006, and the M.Sc. degree in electrical engineering from Shahed University, Tehran, in 2009. He is currently pursuing the Ph.D. degree in electrical engineering with Kansas State University, Manhattan, KS, USA. He has also been involved with telecommunication industry leaders, such as Huawei and Ericsson. His research

interests include artificial inelegance, machine learning, signal processing, wireless communication, cellular networks, and estimation and detection theory.



SOLMAZ NIKNAM received the B.Sc. degree (Hons.) in electrical engineering from the Shiraz University of Technology, Shiraz, Iran, in 2010, the M.Sc. degree in electrical engineering from the Iran University of Science and Technology, Tehran, Iran, in 2012, and the Ph.D. degree from Kansas State University, Manhattan, KS, USA, in 2018. During her Ph.D. degree, she was a recipient of the Kansas Ph.D. Student's Fellowship. She is currently a Postdoctoral Associate

with the Bradley Department of Electrical and Computer Engineering, Virginia Tech. Her research interest includes wireless communication with an emphasis on heterogeneous networks, 5G mmWave networks, and machine learning/artificial intelligence in communication.



BALASUBRAMANIAM (BALA) NATARAJAN (M'97–SM'08) received the B.E. degree (Hons.) in electrical and electronics engineering from the Birla Institute of Technology and Science, Pilani, India, in 1997, and the Ph.D. degree in electrical engineering from Colorado State University, Fort Collins, CO, USA, in 2002. Since 2002, he has been a Faculty Member with the Department of Electrical and Computer Engineering, Kansas State University, Manhattan, KS, USA,

where he is currently the Clair N. Palmer and Sara M. Palmer Endowed Professor and the Director of the Wireless Communication and Information Processing Research Group. He has authored over 150 refereed journal and conference articles along with a book entitled *Multi-Carrier Technologies for Wireless Communications*. He holds a patent in customized spreading sequence design algorithm for CDMA systems. His current research interests include statistical signal processing, stochastic modeling, and optimization theory as applied to wireless communications, sensor networks, biomedical, and cyber-physical systems. He serves as an Editor of multiple journals, including the IEEE TRANSACTIONS ON WIRELESS COMMUNICATIONS and the IEEE TRANSACTIONS ON VEHICULAR TECHNOLOGY.



ALEXEI V. NIKITIN received the Ph.D. degree in physics from the University of Kansas, in 1998. He led R&D work focused on methods and tools in nonlinear signal processing at several startup companies specializing in applications in communications, power electronics, navigation, geophysical sciences, neurology, and biometrics. He is a Co-Founder and the Chief Science Officer of Nonlinear LLC, Wamego, KS, USA. He currently holds 27 U.S. patents.